INTERNATIONAL JOURNAL OF AUTOMOTIVE AND MECHANICAL ENGINEERING
ISSN: 2229-8649 e-ISSN: 2180-1606
VOLUME 22, ISSUE 3, 2025, 12713 - 12724
DOI: https://doi.org/10.15282/ijame.22.3.2025.14.0971

RESEARCH ARTICLE

Battery Simulation Using the NTGK Model: Effects of Model Parameters and Implementation under Dynamic Current Profiles

Melih Yıldız*, Ahmet Aktürk

Faculty of Engineering, Department of Mechanical Engineering, Iğdır University, 76000 Iğdır, Türkiye

ABSTRACT – With the growth in electric powertrain vehicles, the demand for batteries is increasing. Therefore, it is crucial to operate the battery system within an optimum range in terms of performance, life, and safety. In this regard, battery thermal management systems have garnered significant attention for their crucial role in maintaining a battery system within predetermined thermal conditions. The current study focuses on battery simulation using the Newman, Tiedemann, Gu, and Kim (NTGK) model, which is widely applied in the literature. However, the accuracy of this model strongly depends on the empirical parameters U and Y, and existing fitting-based methods often lead to limited reliability. Thus, the effects of the parameters on the temperature evolution of a battery cell were investigated by comparing simulation results with manufacturer data at different discharge rates. This study presents a structured solution scheme to determine the U and Y parameters (for DoD < 0.83). The battery model with the calculated parameters was also simulated under a dynamic current profile representing the Worldwide Harmonized Light Vehicle Test Cycle (WLTC), which is used in approval tests of electric vehicles, at different convective heat transfer coefficients. The results show that temperature prediction with the solution scheme is in good agreement with the battery data obtained from its datasheet. The Y parameter in the NTGK model is of great importance for the development of heat generation characteristics, which in turn affects temperature development. The maximum temperature increase under WLTC was found to be 3.08°C at 20 W/m²K and 8.87°C at 5 W/m²K, while the absolute temperature prediction errors remained below 2.67 K. The temperature rise under dynamic load is consistent with the literature, supporting the validity of the proposed solution scheme.

ARTICLE HISTORY
Received : 04th Dec.2024
Revised : 09th July 2025
Accepted : 01st Aug. 2025
Published : 19th Sept. 2025

KEYWORDS
Li-ion battery
NTGK model
Battery simulation
Temperature variation
Driving cycle

1. INTRODUCTION

Lithium-ion batteries (LIBs) are currently the most frequently used energy storage systems in electric vehicles due to their outstanding energy and power densities. They play a critical role in sustainable transportation and meeting global energy demands [1]. However, limited calendar life, negative effects of cell temperature, and operational insecurity are critical obstacles that must be overcome in the application. Eliminating these drawbacks and providing better performance, longer lifespan, and a higher level of safety for Li-ion batteries is possible through well-designed battery thermal management systems (BTMSs) [2]. In the context of the rapid growth of electric vehicles and the global energy transition, the implementation of advanced battery thermal management systems is essential to support their widespread adoption and ensure reliable performance [3].

For adequate and effective thermal management, it is essential to address the impact of temperature on lithium-ion batteries. In this regard, recent studies have emphasized that maintaining cell temperatures within the range of 15–35 °C and minimizing inter-cell temperature differences ($\Delta T < 5$ °C) are critical for preserving battery performance, ensuring safety, and preventing long-term degradation [4]. While a general operating range of −20 to 60 °C is accepted [5], performance degrades rapidly outside this range. Prolonged exposure to temperatures above 50°C during cycling or storage significantly accelerates capacity fade and power reduction, ultimately leading to thermal runaway [6, 7]. These effects emphasize the pivotal role of precise temperature regulation in minimizing degradation, ensuring safety and optimizing battery longevity. To enhance battery performance and durability, it is crucial to systematically analyze the impact of temperature ranges, progressing from a general overview to a more detailed and focused examination. [8].

To simulate thermal behavior and design parameters for thermal management systems, advanced predictive tools are required. The advanced battery models function as the fundamental prediction tool for assessing battery thermal and electrical performance in various charging and discharging operations. This simulation method reduces both the duration and expenses needed for experimental testing. [9]. Nevertheless, the fact that LIBs contain multiple domains with various physical structures and different thermophysical properties makes the modeling of LIBs more complex [10]. MSMD battery models address these physical problems optimally by implementing their multi-scale, multi-domain framework, which integrates electro-thermal-chemical and empirical models [11]. The MSMD models contain multiple sub-models, which researchers employ in their studies. The P2D model, which Newman proposed, functions as a theoretical model

***CORRESPONDING AUTHOR | Melih Yıldız** | ✉ melih.yildiz@igdir.edu.tr

for simulating lithium-ion distribution between electrode solids and electrolyte liquids while performing electrochemical reactions. The P2D model combines concentrated solution theory with porous electrode theory but requires additional parameters and longer computation times compared to other models [12]. Chen developed the Equivalent Circuit Model (ECM) for simulating battery electrical behavior [13]. The model uses two capacitors with three resistors to solve electrical circuit equations for generating voltage and current curves based on SOC [14]. The values of the resistors and capacitors on the electrical circuit are determined by curve-fitting the experimental data [10]. Lastly, the Newman, Tiedemann, Gu, and Kim model, called the NTGK model, allows for eliminating the physical complexity with its semi-empirical expression. Although the NTGK model has a simple approach, it estimates both electrical and thermal behaviors, the volumetric current transfer, and heat generation in a cell, with lower computational cost [15, 16]. Kwon et al. [17] first suggested the mathematical model of the NTGK approach for a lithium polymer battery, and Kim et al. [18] presented the NTGK model of the Li-ion battery with 14.6 Ah capacity at different current rates and environmental temperatures. The model parameters, U and Y, are derived from discharge characteristics at various depths of discharge and are defined through polynomial fitting. Accurate prediction requires multiple test cycles and high-order fitting for reliable parameter curves. When properly identified, these parameters enable the NTGK model to function as an efficient and accurate thermal simulation tool for batteries.

Several studies have demonstrated the reliability of the NTGK model for thermal applications. In the study [19], it is reported that by using the NTGK model, low root-mean-square errors of 0.3°C at 0.5 C, 0.8°C at 1 C, and 1.3°C at 1.5 C, as well as strong performance under dynamic profiles such as HWFET, are obtained. Further supporting its accuracy, another study [20] demonstrated that the NTGK model achieved an impressive error margin of only 1.2% for discharge rates of 0.5C, 1C, and 2C. Due to its accuracy and efficiency, the NTGK model has been widely adopted in the literature to simulate cooling strategies and designs across single cells, modules, and even battery packs. For example, Chen et al. [21] utilized the NTGK submodel to examine the thermal behavior of the battery under constant discharge currents and various driving cycles (FTP75, NEDC, WLTC), focusing on the impact of busbar dimensions and materials. Similarly, Yıldız et al. [22] employed the NTGK model to assess temperature variations in a cylindrical Li-ion battery (18650 series) under transient current profiles (FTP-72, WLTC, NEDC). Their simulations, validated against manufacturer data and scaled to a 6A current limit, identified FTP-72 as the most demanding profile, with a peak temperature rise of 5.721K. Yetik and Karakoc [23] further demonstrated the model's utility by simulating a 10-cell prismatic module under varying air velocities, temperatures, and C-rates, and then applied Artificial Neural Networks (ANN) for rapid data prediction, finding that silver busbars minimized module temperatures. Çelik et al. [24] validated the robustness of the model by simulating discharge rates of 0.5 C, 1 C, and 1.5 C at 0°C and 25°C, concluding that it accurately predicts thermochemical properties. The model's versatility extends to larger-scale applications, as demonstrated by Ho et al. [25], who applied a 3D thermal-electrochemical NTGK model to a 52.3Ah module and examined discharge rates, fan positioning, and cooling efficiency. Their results demonstrated a 55% reduction in maximum temperature at 5°C with optimized fan circulation. Paccha-Herrera et al. [19] compared the NTGK model with bulk and 3D CFD approaches for 26650 Li-ion cells, highlighting its superiority in simultaneously resolving temperature, voltage, and heat generation. However, as emphasized by [26], it is worth noting that the model's experimental parameters (U and Y) play a decisive role in achieving reasonable accuracy.

Although numerous battery simulation studies are based on the NTGK model, research on determining U and Y parameters and understanding their effects is limited. The current study, therefore, deals with the NTGK battery model for the thermal behavior of a cylindrical battery cell. This research addresses the critical need for a more robust and efficient structured solution scheme for determining the empirical parameters U and Y, which are crucial for accurate NTGK model predictions, thereby overcoming the limitations of conventional fitting methods that can be prone to inaccuracies. The calculated parameters were compared to those estimated with the Ansys Fluent NTGK parameter estimation tool, which is commonly used. Adopting the parameters in the NTGK model, the thermal behavior of the cell was evaluated by comparing the temperature variations at different current rates (C-rates) presented by the manufacturer's data sheet [27]. Besides, the model was simulated for varying current profiles of the Worldwide Harmonized Light Vehicles Test Cycle (WLTC) [28] by considering a maximum allowable current of 6 A. This work demonstrates a real-world application of the proposed method by validating the model's predictions against experimental data provided by the manufacturer's datasheet and simulating a dynamic driving cycle (WLTC), showcasing its practical utility in battery thermal management design.

2. METHODS AND MATERIAL

In this study, 18650 types of cylindrical Li-ion battery cells, whose specifications are given in Table 1, were simulated at different constant current values and dynamic load. The geometric model was created in three dimensions for the calculation domain. Considering the battery characteristics of discharge voltage curves, the NTGK model parameters were numerically determined. With the model parameters, the NTGK battery model was implemented by using the Ansys Fluent software based on the finite-volume method to discretize the solution domain.

Table 1. Battery specifications [27]

Capacity	Minimum	3350 mAh
	Typical	3450 mAh
Nominal voltage		3.6 V
Charging	Voltage	4.2 V
	Current	1475 mA
	time	270 min.
Energy density	Volumetric	693 W/l
	Gravimetric	224 W/kg
Weight		48 g (max.)

2.1 Geometric Model and Meshing

The battery cell geometry has a solid cylindrical shape with dimensions of 65 mm in height and 18 mm in diameter. As seen in Figure 1, the model consists of three domains: the active zone, negative zone, and positive zone. The geometry was meshed with hexahedral and tetrahedral elements for the active zone, positive and negative zones, respectively. For the accuracy of the simulation, mesh dependency studies were conducted by varying the grid spacing from 0.25 mm to 0.5 mm, resulting in a range of 355155 to 1569429 elements. As given in Table 2, the maximum temperature difference is only 0.208 ºC, which corresponds to a 0.462 % relative error. The temperature developments are also given in Figure 2 for these meshes. Thus, the mesh number of 355155 was selected to ensure adequate accuracy and save computational time.

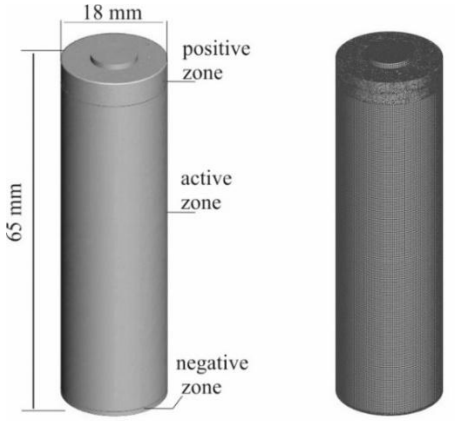

Figure 1. Geometric model and its mesh structure

Table 2. The results of the mesh independence study

Definition	Mesh 1	Mesh 2	Mesh 3	Mesh 4
Spacing (mm)	0.50	0.40	0.30	0.25
Number of mesh elements	355155	569020	1051257	1569429
Maximum temperature at the reference point (ºC)	45.059	44.987	44.896	44.851
Relative difference (%)	-	0.160	0.362	0.462

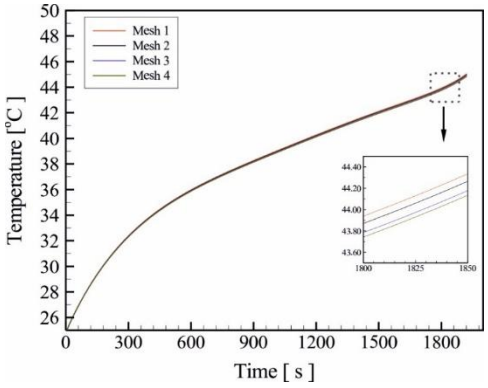

Figure 2. Temperature variations for different mesh elements

2.2 Thermal Model of the Battery Cell

The energy transport equation in a solid region without rotational or translational motion has the following form [29];

$$\frac{\partial}{\partial t}(\rho h) = \nabla.(k\nabla T) + S_h \tag{1}$$

where, T, ρ, and k are temperature, density, and thermal conductivity, respectively. h is the sensible enthalpy as defined in Eq. 2.

$$h = \int_{Tref}^{T} c_p \; dT \tag{2}$$

The second term (S_h) on the right-hand side of Eq. 1 represents the volumetric heat source. In the current study, the heat source generated by the battery due to electrochemical reaction was adopted employing the Newman, Tiedemann, Gu, and Kim (NTGK) model [18].

Firstly, the volumetric current transfer rate (jech) is written as the following expression,

$$j_{ech} = \frac{Q_{nom}}{Q_{ref} Vol_b} Y[U - V] \tag{3}$$

where, Q_{nom} and Q_{ref} denote the nominal and reference capacities of the battery, respectively. Vol_b is the battery volume. V is the potential difference between the positive and negative phases. U and Y are the model parameters. The model parameters, Y and U, are a function of depth of discharge (DoD), and are expressed as follows [19].

$$Y = \left(\sum_{i=0}^{n} a_i (DoD)^n \right) exp\left[-c_1\left(\frac{1}{T} - \frac{1}{T_{ref}}\right)\right] \tag{4}$$

$$U = \left(\sum_{i=0}^{n} b_i (DoD)^n \right) - c_2\left(T - T_{ref}\right) \; where, n = 5 \tag{5}$$

The battery DoD is calculated as follows,

$$DoD = \frac{1}{3600 Q_{nom}} \int_0^t I(t)\, dt \tag{6}$$

Y relates to the internal resistance of the cell, and it is calculated as the inverse of the slope of the voltage-current curves at each DoD. Besides, U represents the open circuit voltage, and it corresponds to the intercept of the voltage-current curve at each DoD value [10, 31].

The current study proposed a specific process for Y and U parameters, considering the volumetric density (Jech) as a homogeneous assumption, meaning the ratio of current to the cell volume. Thus, the following equation expressed by j is obtained.

$$j = I\frac{Q_{ref}}{Q_{nom}} = Y[U - V] \tag{7}$$

Since the Y and U values at any DoD value equal those of different current loads, an algebraic equation system can be established for each Y and U at a certain DoD as follows.

$$\begin{aligned} j_{i,1} &= Y_i U_i - Y_i V_{i,1} \\ j_{i,2} &= Y_i U_i - Y_i V_{i,2} \\ &\vdots \\ j_{i,c} &= Y_i U_i - Y_i V_{i,c} \end{aligned} \tag{8}$$

In Eq. 8, *i* and *c* denote a DoD level and the number of different current loads (for example, 2A, 4A, and 6A, thus c=3), respectively. V_i is the battery voltage as a function of DoD for each load, and is obtained from battery characteristic curves or experiments. The equation system has two unknowns, U_i and Y_i, at each i-th DoD level, and the calculation of the unknowns is given below.

$$Y_i = \frac{\left(\sum_{k=2}^{c} j_{i,k}\right) - (c-1) j_{i,1}}{(c-1) V_{i,1} - \sum_{k=2}^{c} V_{i,k}} \tag{9}$$

By substituting Eq. 9 into any algebraic equation in the equation system (Eq. 8), the U_i is easily estimated. With the calculated U_i and Y_i as a function of DoD, the coefficients, a_i and b_i stated in Eq.4 and Eq. 5 were determined using the curve fitting least square method. A program was coded in MATLAB environment with the procedure briefly presented in Algorithm 1. The calculated coefficients by the structural solution scheme and by using the estimation tool for the NTGK model in ANSYS-Fluent are presented in Table 3.

Algorithm 1. Determination of coefficients of the U and Y parameters for the NTGK battery model

1: **Input: D_1 (time, V_1 , I_1), …D_c(time, V_c , I_c), Q_{ref}** ⇨ real voltage and current data, and the reference capacity
2: **output: A(a_0, a_1, …a_5), B(b_0, b_1, …b_5)** ⇨ polynomial coefficients in Eqs. 4 and 5
3: Load real voltage and current data D={D_c}
4: **for** each data D_c **do** ⇨ calculation of Q_{nom} and DoD values using Eq. 6
5: **end**
6: select **DoD** interval
7: **for** each DoD values **do** ⇨ arrangement of $V_{i,c}$ and $J_{i,c}$ in Eq. 7 vectors for each current state, I_1, … I_c
8: **end**
9: **for** each DoD values **do** ⇨ calculation of Y_i and U_i using Eq. 9
10: **end**
11: **Procedure** the curve fitting to the calculated Y_i and U_i
using Matlab built-in function, `lsqcurvefit`
with "`Levenberg-Marquardt`" option
12: Plot the calculated Y_i and U_i curves with their fitting curves versus DoD
13: Obtain A and B vectors

Table 3. The estimated coefficients of U and Y parameters

Method	U coefficients					
	a_0	a_1	a_2	a_3	a_4	a_5
The proposed method	4.1817	-2.4311	12.0556	-38.4202	52.1143	-24.9433
The tool estimation	4.1846	-2.1768	8.6493	-25.9732	34.6307	-16.5845
	Y coefficients					
	b_0	b_1	b_2	b_3	b_4	b_5
The structured solution scheme	17.86	49.77	-41.21	-280.00	554.40	-291.40
The tool estimation	18.82	83.88	-351.43	782.45	957.03	461.89

The electrochemical reaction heat, which is S_h in Eq. 1, is calculated with Eq. 10.

$$S_h = \dot{q}_{Ech} = j_{ech}\left[(U - V) - T\frac{dU}{dT}\right] \tag{10}$$

In Eq. 10, the first term is irreversible heat due to internal resistance of the cell, and the second term is reversible heat from the electrochemical reaction in the cell [25].

For a constant specific heat (cp), density (ρ), and thermal conductivity (k), substituting Eq. 10 into Eq. 1 as well, the expression Eq. 11 is obtained. The defined materials and their physical properties for each zone are given in Table 4 [19, 30].

$$\rho C_P \frac{\partial T}{\partial t} = \nabla.(k_n \nabla T) + j_{ech}(U - V) - j_{ech} T \frac{dU}{dT} \tag{11}$$

Table 4. Materials and properties of active, negative, and positive zones

Zone	Material	k [W/mK]	Cp [J/kg K]	ρ [kg/m^3]
Active	NCA/(Graphite+SİOx)	k_r = 0.25 $k_\theta = k_z$ =30	1261	2500
Positive	aluminium	202.4	871	2710
Negative	steel	16.27	502	8930

Having built in the geometric and mathematical models for the battery, the numerical analyses were performed for both cases of U and Y given in Table 3. The battery cut-off voltage was set to 2.7 V, and the simulations were carried out up to the time when the battery reached the cut-off voltage at 2A, 4A, and 6A for different convective heat transfer coefficients at a free stream temperature of 25°C. Besides, the battery was analyzed under a variable current profile. The variable current profile was first created over an electric vehicle operated under the Worldwide Harmonized Light-Duty Test Cycle-class 2 (WLTC-class2), simulated by the ADVISOR program [31,32]. Finally, the scaled current profile was attained as illustrated in Figure 3 by scaling the current profile at a maximum of 6.0 A, disregarding regeneration. Table 5 summarizes the cases in the numerical study.

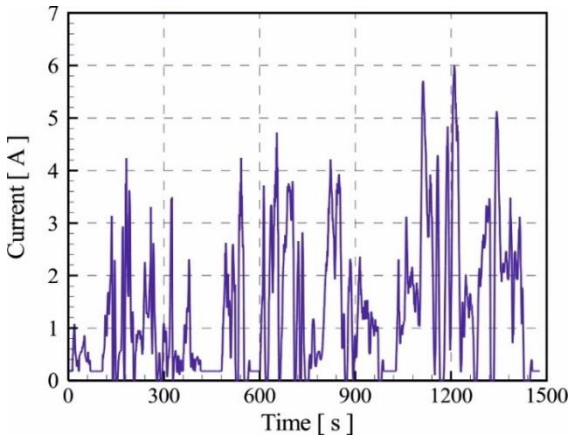

Figure 3. Scaled current profile under the WLTC-class2

Table 5. The cases of the simulations performed in the current study

The NTGK model	Current load for discharge			
	2 A	4 A	6A	Dynamic current profile
Calculation method of U and Y parameters	The structured solution scheme estimation-tool	The structured solution scheme estimation-tool	The structured solution scheme estimation-tool	The structured solution scheme
Boundary condition	Convective heat transfer with h=15Wm^{-2} K Tamb = 25 ºC	Convective heat transfer with h=20Wm^{-2} K Tamb = 25 ºC	Convective heat transfer with h=20 Wm^{-2} K Tamb = 25 ºC	Convective heat transfer with h=5,10, 15, and 20 Wm^{-2} K, Tamb = 25 ºC

3. RESULTS AND DISCUSSION

In this section, it is presented that the NTGK model with the structured solution scheme has predictive capabilities and reveals important findings about how empirical parameter accuracy affects thermal simulation reliability under practical load conditions. This section, firstly, presents the obtained U and Y parameters and total heat generation variation. Secondly, the voltage curves and temperature variations during discharge periods at different current loads are provided for both the U and Y calculation methods to verify the battery model. Lastly, the results of dynamic current loads are evaluated.

3.1 The U and Y Parameters and Total Heat Generation

Figure 4 illustrates the U and Y parameters determined by both the presented methods in the current (Eq.s 7-9) and the parameter estimation tool of ANSYS-Fluent. It can be seen that the calculated U parameters, depending on DoD, are compatible with each other. On the other hand, although the Y parameters have the same variation characteristics up to nearly 0.80 DoD, the curve characteristics differ after this DoD value. This discrepancy arises because the calculation range is restricted to DoD < 0.83. Beyond this threshold, U and Y parameters exhibit high error rates. The limitation may bring about over-prediction beyond the range of the curve fitted [26].

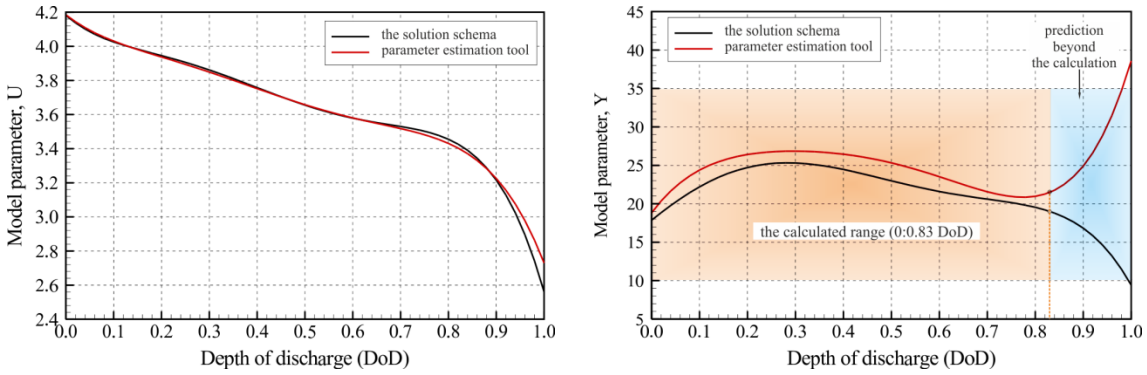

Figure 4. Comparison of U and Y parameters determined by two methods

Considering the variation parameters beyond the calculation range, two curve characteristics arose sharply increasing trend with the parameter estimation tool and an exponentially decreasing trend with the structured solution scheme in the current study. Therefore, it can be expected that the difference in the temperature prediction since the heat generated by the cell relies on the Y parameters along with U in the NTGK model, as mentioned before.

Figure 5 shows the heat generation curves at different current loads for the two methods of U and Y calculations. As can be seen in this figure, the heat generation curve characteristics change with adverse trends in the Y curves. The heat generation values decrease when the Y value increases. Conversely, lower Y values correlate with higher heat generation (see Figure 4). Therefore, in the case of the presented method, the heat generation values increase while they decrease in the estimation tool. It should also be noted that the heat generation characteristics for discharge and charge periods are expected to be those obtained at the presented method [33, 34]. Considering the effect of current load on heat generation values, the increase in current elevated the total heat generation involving both irreversible and reversible heat [35].

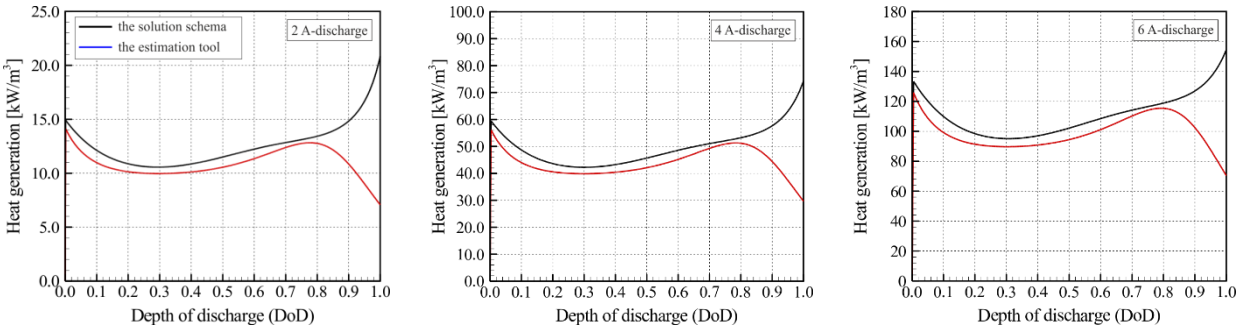

Figure 5. Comparison of the total heat generation variations for two methods at different constant current loads

The results show that the parameter Y has a greater influence on total heat generation than U, especially at higher depth of discharge levels, where resistive losses are more significant. This behavior is consistent with the thermodynamic basis of heat generation, where the irreversible Joule heating is primarily governed by Y. Thus, even small deviations in Y can lead to significant differences in thermal predictions. Therefore, a more accurate determination of Y through the structured scheme ensures better alignment with actual battery behavior.

3.2 The Validation of the Battery Model

As mentioned before, the NTGK model allows predicting both electrical and thermal characteristics. Therefore, the voltage-time curves and temperature values obtained from the simulation results were compared to the battery characteristics presented by the manufacturer [27] to validate the methods based on the NTGK model.

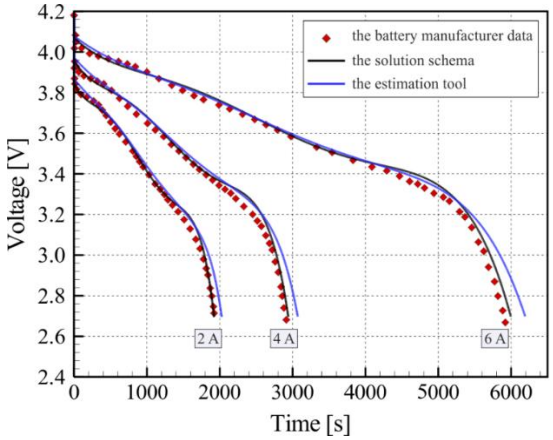

Figure 6. Comparison of voltages at different constant current loads

Figure 6 shows the comparison of the voltage time curves taken from the manufacturer's data sheet and the simulation results for 2, 4, and 6 A constant current values. The upper cut-off voltage is 4.2 V and the lower cut-off voltage is 2.7 V. As can be seen in the figure, the voltage curves obtained from both methods are compatible with the battery manufacturer's data. However, in the case of the estimation tool, the voltage curves exhibit slight deviations after sharply decreasing trends for all current loads, which increases the simulation time because they do not reach the cut-off voltage.

Figure 7 illustrates the temperature profiles obtained with the NTGK models and provided by the battery manufacturer's datasheet. The figure shows that the predicted temperatures are in good agreement with the actual battery data for certain periods under each current load. However, the temperatures partially deviate from the temperature profile of the battery data after those times. Moreover, in the case of the estimation tool, the temperature profile curves follow downward after those times, in contrast to others. The reason for this is due to the heat generation profiles obtained at the NTGK model with the estimation tool. Considering the absolute errors of the predicted temperature during discharge times, the errors at 2 A range from 4.10^{-4} to 0.194 K for the presented method and from 0.08 to 0.372 K for the estimation tool, up to 4995 seconds. After that time, the errors range from 0.72 to 2.67 K for the presented method and from 1.01 to 3.66 K for the estimation tool.

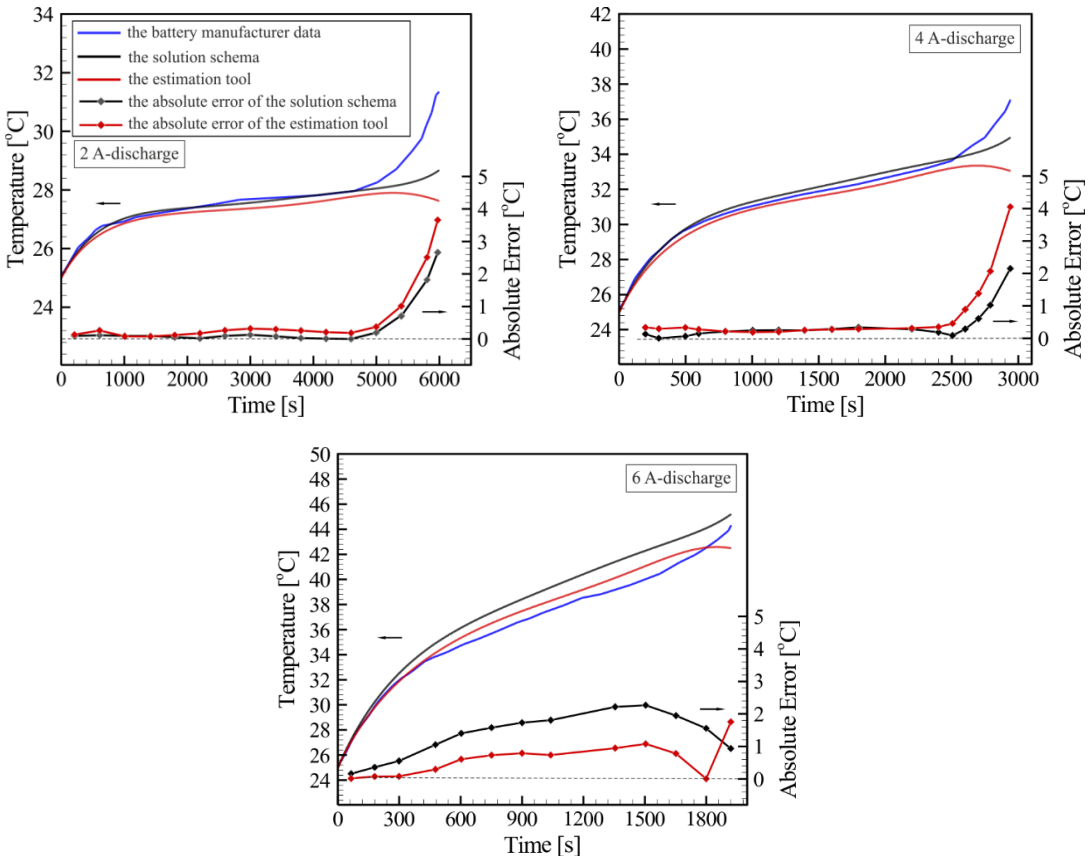

Figure 7. Comparison of temperature values and their errors at different constant current loads

Similarly, at 4 A, the errors remain quite low up to around 2500 s, after which they increase to 2.15 K for the presented method and 4.05 K for the estimation tool. This shows that the NTGK model with the presented method provides more accurate predictions compared to the estimation tool. Conversely, at 6 A, the predicted temperature with the estimation tool shows better agreement with the temperatures of the battery data than the presented method. However, the errors with the presented method are at a reasonable level, and the temperature curve characteristics are more compatible with those of battery data.

3.3 The Battery Simulation under Dynamic Current Profile

In the analysis of the battery under the driving cycle, the U and Y coefficients obtained with the current solution scheme were used. For the cylindrical battery simulation, the nominal cell capacity and reference capacity were set to 3.45Ah. The initial depth of discharge (DoD) was selected as 0, which means full capacity. Figure 8(a) shows six consecutive speed/time profiles of the WLTC-class-2 driving cycle, taking 1478 seconds. Additionally, Figure 8(b) shows the corresponding scaled-current/time profile along with the state of charge (SOC) to which the battery is subjected in the simulation. As can be clearly seen from Figure 8(b), the maximum discharge current value is 6A while the minimum current value is 0A. Besides, the current drawn from the battery reduces the SOC value starting from 100% to approximately 6% over time.

During the simulation, the voltage/time profile created under the current profile of the driving cycle is given in Figure 9. In the figure, the maximum voltage value is approximately 4.18 V at the beginning of the simulation, and the minimum voltage value is around 2.79 V at the 8733rd second. The discharge current value during the emergence of the minimum voltage is 5 A. From the moment the minimum battery potential was encountered, the discharge current values remained below 5 A and experienced various decreases and increases. For this reason, the battery potential fluctuated until the 8868th second and remained above 2.79 V.

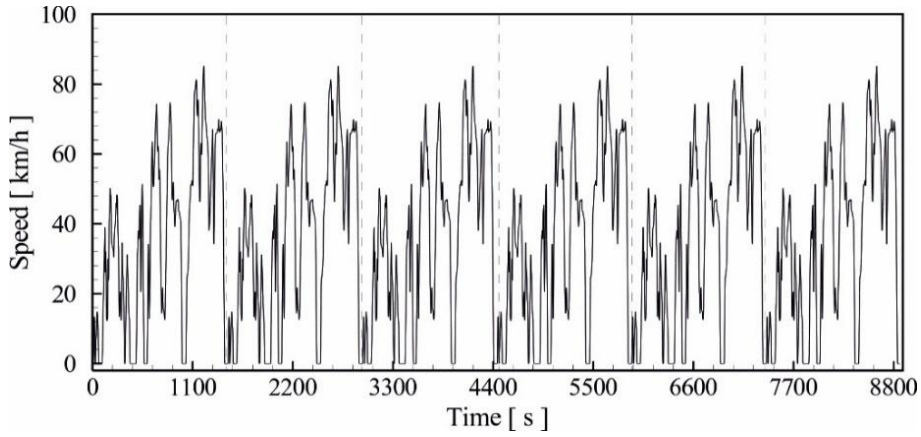

(a)

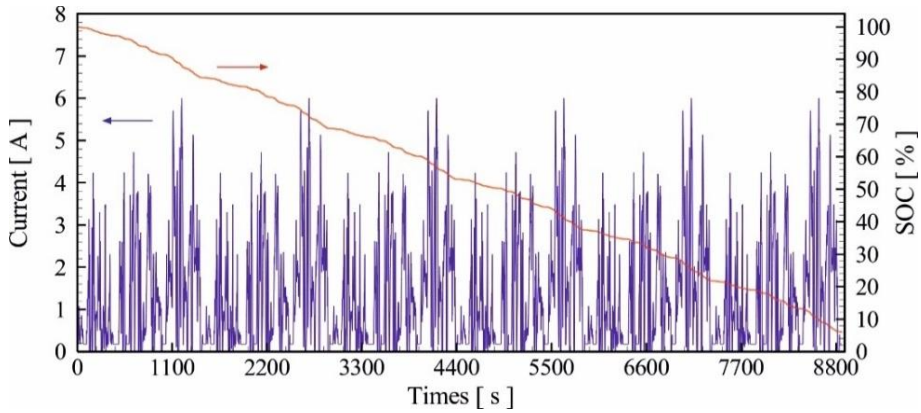

(b)

Figure 8. (a) The speed profile of the successive WLTC-class2; (b) the scaled current profile over the cycle period

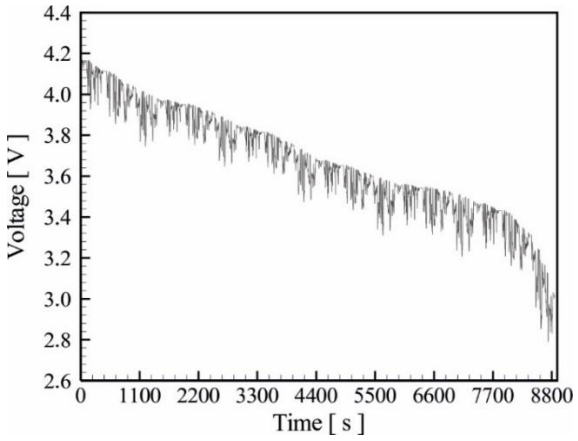

Figure 9. The voltage variation under the WLTC-class2

Figure 10(a) displays the total heat generation profile of the battery during the driving cycle. Six distinct peaks correspond to the maximum heat generation points for each WLTC driving cycle. The peak values of the heat generation emerged because of the clustering of successive 5 A and 6 A discharge currents in a certain region. These clustered higher discharge currents can be obviously monitored from the current profile in Figure 8, as well. It should also be noted that the peak values for each recurrence cycle increase due to decreasing SOC level, in other words, increasing DoD level. This is because the heat generation depends on both current and state of charge or depth of discharge of the battery [33]. Figure 10(b) shows the temperature increase starting from 25°C ambient temperature for various convective heat transfer coefficients, h = 5, 10, 15 and 20 W / m^2 K under the driving cycle. By examining the temperature curves, it can be stated that the effect of heat transfer coefficients is not obvious during the first 600 seconds since the battery temperature was initially at ambient temperature values, and the heat transfer rate from the battery wall remains very low until more heat is released from the cell.

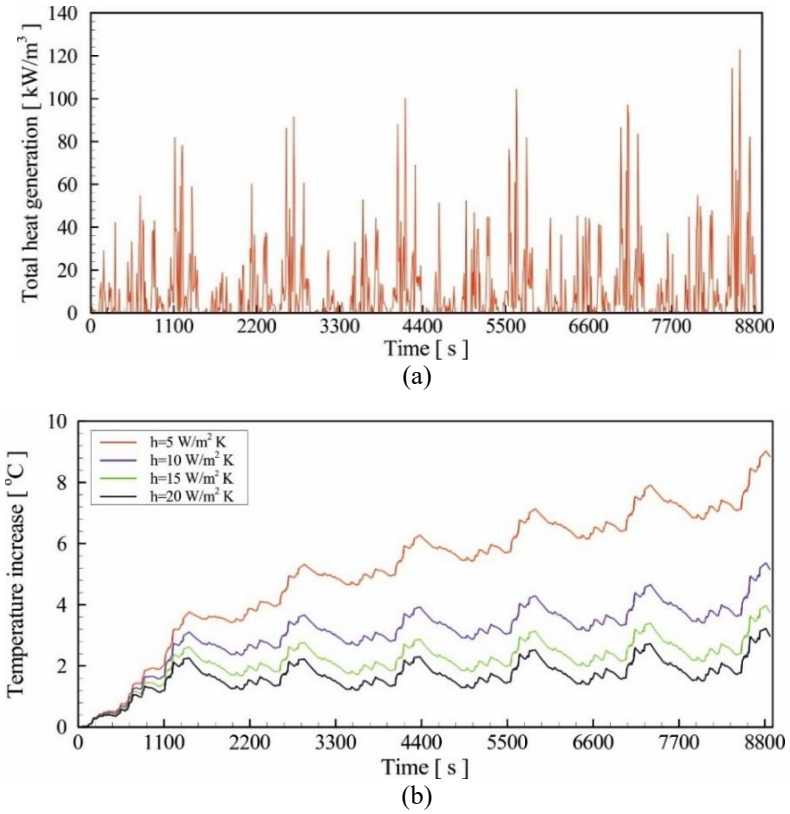

Figure 10. (a) The total heat generation, and (b) the surface temperature increases at different heat transfer coefficients

Thus, the effect of the convective heat transfer coefficient on temperature values becomes significant over time. As expected, increasing the heat transfer coefficient maintained the battery temperature lower due to increasing the heat transfer rate from the wall to the ambient. Consequently, the temperature rise at the end of the cycle is 3.08°C at 20 W/m^2K, while it is 8.87°C at 5 W/m^2K. Liu et al. [36] reported that the temperature increase is 3.29 K for a 20 Ah lithium-ion polymer battery cell with air cooling under the driving cycle consisting of consecutive WLTC cycles, and considering regenerative braking. Besides, Daud et al. [37] carried out a study on predicting battery temperature over the New European Driving Cycle (NEDC), and they found that the temperature increase is 1.5 K for only one cycle period without regenerative braking. Considering these results, the simulation results in the current study can be regarded as reasonable.

The model demonstrates its practical use for thermal management system design through its ability to predict thermal behavior during realistic drive cycles such as WLTC with a maximum temperature increase of 8.87°C. The optimal operating temperature range for lithium-ion batteries is between 15°C and 35°C to maintain performance, extend life, and ensure safety [4]. The battery stays within its optimal operating range when the temperature increases by less than 9°C from an ambient temperature of 25°C during dynamic load conditions.

4. CONCLUSIONS

The NTGK battery model commonly used in battery simulation studies was numerically investigated to reveal the effect of the model parameters, U and Y, on the results. The structured solution scheme was presented for the calculation of U and Y parameters. The battery cell was also simulated by the NTGK model with the U and Y parameters calculated by the presented solution scheme under dynamic current loads representing the WLTC-class 2 driving cycle with a 6 A maximum allowable current. Based on the results, the main findings can be stated as follows.

- The presented solution scheme for calculating U and Y parameters is as reliable as the calculation values by the estimation tool, since the presented method provided slightly more accuracy of the results.
- The study precisely reveals that Y is the decisive parameter for heat generation characteristics, causing battery temperature development characteristics during discharge periods. The development of reliable battery thermal models requires an accurate solution scheme to determine empirical parameters, especially 'Y', because this information enables precise real-world battery behavior prediction and effective BTMS design.
- The temperature rises under the driving cycle consisting of 6 successive WLTC cycles varied between 3.08°C and 8.87°C, depending on the convective heat transfer coefficient, clearly demonstrating that higher convective heat transfer coefficient (h) values lead to significantly reduced temperature increases, thereby crucially enhancing battery safety and overall operational reliability in BTMS design.

ACKNOWLEDGEMENTS

This study was not supported by any grants from funding bodies in the public, private, or non-profit sectors.

CONFLICT OF INTEREST

The authors declare no conflicts of interest.

AUTHORS CONTRIBUTION

M. Yıldız (Conceptualization; Methodology; Validation; Formal analysis; Investigation; Software; Visualization; Writing - original draft; Writing - review & editing)

A. Aktürk (Methodology; Validation; Formal analysis; Data curation; Investigation; Software; Writing - original draft; Writing - review & editing;)

REFERENCES

[1] K. R. Ngoy, V. T. Lukong, K. O. Yoro, J. B. Makambo, N. C. Chukwuati, C. Ibegbulam, et al., "Lithium-ion batteries and the future of sustainable energy: A comprehensive review," *Renewable and Sustainable Energy Reviews*, vol. 223, p. 115971, 2025.

[2] H. Liu, Z. Wei, W. He, and J. Zhao, "Thermal issues about Li-ion batteries and recent progress in Battery Thermal Management Systems: A review," *Energy Conversion and Management*, vol. 150, pp. 304–330, 2017.

[3] S. M. Naiek, S. Aungsuthar, C. Harper, and C. Hendrickson, "Battery electric vehicle safety issues and policy: A review," *World Electric Vehicle Journal*, vol. 16, no. 7, p. 365, 2025.

[4] E. Tosun, S. Keyinci, A. C. Yakaryilmaz, and M. Ozcanli, "A study on the removal of heat generated by a lithium-ion battery module: A fan-assisted battery cooling approach," *Processes*, vol. 13, no. 3, p. 848, 2025.

[5] A. Väyrynen and J. Salminen, "Lithium-ion battery production," *Journal of Chemical Thermodynamics*, vol. 46, pp. 80–85, 2012.

[6] S. Wang, T. Wu, H. Xie, C. Li, J. Zhang, L. Jiang, et al., "Effects of current and ambient temperature on thermal response of lithium-ion battery," *Batteries*, vol. 8, no. 11, p. 203, 2022.

[7] C. Li, Y. Ding, Z. Zhou, Y. Jin, X. Ren, C. Cao, et al., "Parameter optimization and sensitivity analysis of a lithium-ion battery thermal management system integrated with composite phase change material," *Applied Thermal Engineering*, vol. 228, p. 120530, 2023.

[8] S. S. Madani, Y. Shabeer, F. Allard, M. Fowler, C. Ziebert, Z. Wang, et al., "A comprehensive review on lithium-ion battery lifetime prediction and aging mechanism analysis," *Batteries*, vol. 11, no. 4, p. 127, 2025.

[9] M. Mama, E. Solai, T. Capurso, A. Danlos, S. Khelladi, and M. Köksal, "Comprehensive review of multi-scale Lithium-ion batteries modeling: From electro-chemical dynamics up to heat transfer in battery thermal management system," *Energy Conversion and Management*, vol. 325, p. 119223, 2024.

[10] A. Abbas, N. Rizoug, R. Trigui, A. Babin, E. Redondo-Iglesias, and S. Pelissier, "Thermal modeling of batteries for EV Energy Management," in *IEEE Conference on Vehicle Power and Propulsion (VPPC),* Merced, CA, USA, 2022, pp. 1–6.

[11] G.-H. Kim, K. Smith, K.-J. Lee, S. Santhanagopalan, and A. Pesaran, "Multi-domain modeling of lithium-ion batteries encompassing multi-physics in varied length scales," *Journal of The Electrochemical Society*, vol. 158, no. 8, pp. A955–A970, 2011.

[12] A. Jokar, B. Rajabloo, M. Désilets, and M. Lacroix, "Review of simplified pseudo-two-dimensional models of lithium-ion batteries," *Journal of Power Sources*, vol. 327, pp. 44–55, 2016.

[13] M. Chen and G.-A. Rincon-Mora, "Accurate electrical battery model capable of predicting runtime and I-V performance," *IEEE Transactions on Energy Conversion*, vol. 21, no. 2, pp. 504–511, 2006.

[14] G. Li, S. Li, and J. Cao, "Application of the MSMD framework in the simulation of Battery Packs," in *ASME 2014 International Mechanical Engineering Congress and Exposition*, Montreal, QC, Canada, 2014, p. IMECE2014-39882.

[15] U. Moralı, "Computational modeling and statistical evaluation of thermal behavior of cylindrical lithium-ion battery," *Journal of Energy Storage*, vol. 55, p. 105376, 2022.

[16] N. Napa, M. K. Agrawal, and B. Tamma, "Design of novel thermal management system for li-ion battery module using metal matrix based passive cooling method," *Journal of Energy Storage*, vol. 73, p. 109119, 2023.

[17] K. H. Kwon, C. B. Shin, T. H. Kang, and C.-S. Kim, "A two-dimensional modelling of a lithium-polymer battery," *Journal of Power Sources*, vol. 163, no. 1, pp. 151–157, 2006.

[18] U. S. Kim, J. Yi, C. B. Shin, T. Han, and S. Park, "Modeling the dependence of the discharge behaviour of a lithium-ion battery on the environmental temperature," *Journal of The Electrochemical Society*, vol. 158, no. 5, pp. A611–A618, 2011.

[19] E. Paccha-Herrera, W. R. Calderón-Muñoz, M. Orchard, F. Jaramillo, and K. Medjaher, "Thermal modeling approaches for a $LiCoO_2$ lithium-ion battery—a comparative study with experimental validation," *Batteries*, vol. 6, no. 3, p. 40, 2020.

[20] O. Yetik, U. Morali, and T. H. Karakoc, "A numerical study of thermal management of lithium-ion battery with nanofluid," *Energy*, vol. 284, p. 129295, 2023.

[21] H. Chen, T. Zhang, Y. Hua, Q. Gao, Z. Han, K. Yang, et al., "Simulation study on the interaction between the battery module and busbar under typical driving conditions of electric vehicles," *Case Studies in Thermal Engineering*, vol. 45, p. 103006, 2023.

[22] M. Yıldız and A. Aktürk, "A CFD-based study on a Li-ion battery temperature variation under the electrical current profiles derived from the driving cycles," in *5th International Eurasian Conference on Science, Engineering and Technology (EurasianSciEnTech)*, Ankara, Türkiye, 2024, pp. 1252–1260.

[23] O. Yetik and T. H. Karakoc, "Estimation of thermal effect of different busbars materials on prismatic Li-ion batteries based on Artificial Neural Networks," *Journal of Energy Storage*, vol. 38, p. 102543, 2021.

[24] A. Celik, H. Coban, S. Göcmen, M. A. Ezan, A. Gören, and A. Erek, "Passive thermal management of the lithium-ion battery unit for a solar racing car," *International Journal of Energy Research*, vol. 43, no. 8, pp. 3681–3691, 2019.

[25] V.-T. Ho, K. Chang, S. W. Lee, and S. H. Kim, "Transient thermal analysis of a Li-ion battery module for electric cars based on various cooling fan arrangements," *Energies,* vol. 13, no. 9, p. 2387, 2020.

[26] Y. Zhang, H. Liu, S. Liu, S. Pan, C. Tian, and J. Hu, "Prediction model of thermal behavior of lithium battery module under high charge-discharge rate," *Journal of Energy Storage*, vol. 74, p. 109366, 2023.

[27] Panasonic Corporation, "NCR18650GA Datasheet," [Online]. Available: https://datasheetspdf.com/datasheet-pdf/974430/NCR18650GA.html. Accessed: Dec. 9, 2023.

[28] P. Asef, M. Milan, A. Lapthorn, and S. Padmanaban, "Future trends and aging analysis of battery energy storage systems for electric vehicles," *Sustainability,* vol. 13, no. 24, p. 13779, 2021.

[29] Fluent Inc., *Fluent 6.3 User's Guide,* Lebanon, NH, USA, 2006.

[30] T. T. D. Nguyen, "Understanding and modelling the thermal runaway of li-ion batteries," Ph.D. dissertation, Université de Picardie Jules Verne, France, 2021. NNT:2021AMIE006.

[31] T. Markel, A. Brooker, T. Hendricks, V. Johnson, K. Kelly, B. Kramer, et al., "ADVISOR: A systems analysis tool for advanced vehicle modeling," *Journal Power Sources*, vol. 110, no. 2, pp. 255–266, 2002.

[32] D. R. Robbio, M. C. Cameretti, and E. Mancaruso, "Investigation by modelling of a plug-in hybrid electric commercial vehicle with diesel engine on WLTC," *Fuel,* vol. 317, p. 123519, 2022.

[33] S. Neupane, M. Alipanah, D. Barnes, and X. Li, "Heat generation characteristics of $LiFePO_4$ pouch cells with passive thermal management," *Energies,* vol. 11, no. 5, p. 1243, 2018.

[34] E. Gümüşsu, Ö. Ekici, and M. Köksal, "3D CFD modeling and experimental testing of thermal behavior of a Li-Ion battery," *Applied Thermal Engineering*, vol. 120, pp. 484–495, 2017.

[35] M. Yildiz, H. Karakoc, and I. Dincer, "Modeling and validation of temperature changes in a pouch lithium-ion battery at various discharge rates," *International Communications in Heat and Mass Transfer*, vol. 75, pp. 311–314, 2016.

[36] Y. Liu, Y. G. Liao, and M. C. Lai, "Temperature variations of a lithium-ion polymer battery cell during electric vehicle driving cycles," in *IEEE Transportation Electrification Conference and Expo (ITEC)*, Chicago, IL, USA, 2021, pp. 34–39.

[37] Z. H. C. Daud, S. A. A. Bakar, N. A. Husain, P. M. Samin, and D. Chrenko, "Temperature prediction of lithium-ion battery used in realistic driving cycles," in *2017 IEEE Vehicle Power and Propulsion Conference (VPPC)*, Belfort, France, 2017, pp. 1–4.